Robotica: (2021) volume 39, pp. 1023–1036. © The Author(s), 2020. Published by Cambridge University Press.
doi:10.1017/S0263574720000879

Appraisement and Analysis of Dynamical Stability of Under-Constrained Cable-Driven Lower-Limb Rehabilitation Training Robot

Yan-Lin Wang*, Ke-Yi Wang, Wan-Li Wang, Zhuang Han and Zi-Xing Zhang

College of Mechanical and Electrical Engineering, Harbin Engineering University, Harbin 150001, China

(Accepted August 12, 2020. First published online: September 10, 2020)

SUMMARY

The dynamical stability of the cable-driven lower-limb rehabilitation training robot (CLLRTR) is a crucial question. Based on the established dynamics model of CLLRTR, the solution to the wrench closure of the under-constrained system is presented. Secondly, the stability index of CLLRTR is proposed by the Krasovski method. Finally, in order to analyze the stability distribution of CLLRTR in the workspace, the stability evaluation index in the workspace is calculated using the eigenvalue decomposition method. The stability distribution laws of CLLRTR are further verified by the experimental study. The results provide references for studying trajectory planning and anti-pendulum control of CLLRTR.

KEYWORDS: Rehabilitation; Cable-driven robot; Krasovski method; Wrench enclosure; Dynamical stability.

1. Introduction

The aging of the population, cerebral thrombosis, traffic accidents, and so on lead to an increase in the number of patients with physical movement injuries.[1,2] Medical research data show that effectively improve the ability of the functional movement of the limbs, muscle strength, and coordination of the patients with the motor disorder through the modern medical treatment and task-oriented repetitive motion.[2–5]

In order to better help patients, the field of rehabilitation training robots has attracted a large number of clinicians, therapists, and engineers. It is hoped that some new technologies can be developed to realize the spatial functional movements with the different patient's needs and effectively improve the daily living standards and happiness of the patients. Ming et al.[6] firstly proposed that the cable-driven parallel robot (CDPR) is divided into four categories: (1) when $m = n$, it is an incomplete constrained positioning mechanisms, where m is the number of cables, and n is the number of degrees of freedom (DOF) for the end-effector; (2) when $m = n + 1$, it is a complete constrained positioning mechanisms; (3) when $m > n + 1$, it is a redundant constrained positioning mechanisms; and (4) when $m < n$, it is an under-constrained positioning mechanisms. Because of less constraints, when $m < n$, this kind of robot is relatively few studied. A large number of the works have been carried out on the assisted exoskeleton robot, especially on the lower-limb rehabilitation robot. The rehabilitation of the patients is carried out by simulating the trajectory of the joints of the lower

* Corresponding author. E-mail: wangyanlin0513@21cn.com

limb in the normal walking gait, and it has a good effect on the rehabilitation of the patients.[7] Liu et al.[8] analyzed the dynamic modelling method of the rigid-flexible coupled parallel mechanism. The variation characteristics of the dynamic stress for the flexible components are discussed. Berti et al.[9] proposed an efficient algorithm to solve the direct geometrico-static problem of the under-constrained cable-driven parallel robots based on the interval analysis. The algorithm can find all direct geometrico-static solutions and real solutions with non-negative cable tensions. Yu et al.[10] presented a multi-modal control scheme for rehabilitation robots. Several control schemes have been proposed for robotic exoskeletons driven by series elastic actuators integrated into the controller to guarantee the safety of the patient. The research progress on rehabilitation training methods and its control strategies of CLLRTR are relatively slow at home.[11–14] And the type of training action is single, the space range of motion is relatively small, and the motion of the end-executor is in one same plane. Furthermore, the control methods mainly focus on the speed or position servo control mode. It can't train the muscle strength of the patients, and the training methods are mostly passive training. Khor et al.[15] designed an upper and lower limb hybrid training rehabilitation robot. Both the upper and lower limbs of the patients are subjected to alternating rigid forces, which may cause secondary injury to the patients. ABBASNEJAD designed a CDPR to help rehabilitation training of patient lower limb.[16] But the four cables were distributed in one same plane, so the lower limb can only move in the same plane. It limits the DOF and flexibility of the rehabilitation training. In order to solve the problem that the general external wrench in some parts of the trajectory cannot be balanced, a reconfigurable design of the robot is investigated in which the cable attachment points on the base can move with the motion of the limb in its trajectory. The results show that the area of wrench-closure zones in the trajectory can be increased using different actuation schemes.[16] Considering the coupling of the cable vibrations and the end-effector vibrations, the dynamic stiffness of the CDPR was analyzed. The effects of the changes in cable stiffness on the whole robot were obtained.[17] Yang et al.[18,19] proposed an adaptive controller for a cable-driven parallel rehabilitation robot. The controller with a fuzzy tuner can adjust and optimize the control parameters on the basis of position error. Lamine et al.[20] proposed an algorithm of the CDPR. The algorithm can provide reliable and robust results against rounding error effects. However, the high computation time could be a limiting factor. Kino et al.[21] proposed a CDPR with an active balancer. The method of the approximate trajectory of the balancer was used to estimate load parameters. An adaptive controller was proposed to examine the method. The research results demonstrate the usefulness of the proposed controller through simulation. Lu et al.[22] studied the kinematics and dynamics of novel 3SPU + 2RPU + R type parallel manipulator with a couple-constrained wrench. The study results show that the novel parallel manipulator has a large workspace in any direction. Bosscher et al.[23] presented a calculation method of the stability of the CDPR based on the slope of the motion screw. The method can evaluate the dynamical stability of the CDPR. But the method can't consider the influence of the cable tension on the stability. Nathan Michael et al. analyzed the static stability of the CDPR using the Hessian matrix and discussed spatial configuration. The motion of the CDPR is stable when eigenvalues of the Hessian matrix are positive.[24] Wang[25] analyzed the stability of CDPR by the hybrid force-position-pose approach and presented the stability evaluation index. Behzadipour et al.[26] applied the total stiffness matrix of the system to evaluate the stability. The requirements for the process of the calculation, the total stiffness, and the stability of the system are very strict. It is difficult to quantitatively evaluate the dynamical stability of the system.

The main operated object of CLLRTR is the human lower limb, so it has strict requirements for the dynamical stability of this kind system. This paper proposes an under-constrained cable-driven lower-limb rehabilitation robot that can complete different functional motions in space. The kinemics and dynamics of CLLRTR are analyzed in Section 3. The workspace and optimization method of the cable tensions are discussed in Section 4. According to the Krasovski method, the analysis method and evaluation index of the dynamical stability are introduced in Section 5. And the distribution of the dynamical stability of CLLRTR is analyzed and calculated in Section 6. The experimental results can provide a safe trajectory planning area for different training modes of lower-limb rehabilitation robots.

https://doi.org/10.1017/S0263574720000879 Published online by Cambridge University Press

Table I. The symbols describing the important variables.

Parameter	Meaning	Parameter	Meaning
L_i	Cable length	$\boldsymbol{T}$	Cable tension vector
$[X, Y, Z]^T$	Position of the footplate	$\boldsymbol{T}^*$	Minimal norm solution to the cable tension
$[\varphi_1, \varphi_2, \varphi_3]^T$	Posture of footplate	$\boldsymbol{V}(\boldsymbol{x})$	Lyapunov function
${}^O\boldsymbol{R}_P$	Rotation matrix	$\mathbf{D}$	Eigenvalue matrix of $\boldsymbol{F}(\boldsymbol{x})$
$\boldsymbol{J}_+$	Structure matrix of the system	λ_i	Eigenvalue
$\boldsymbol{J}_w$	Wrench matrix composed of the gravity and inertia forces	S	Dynamical stability index

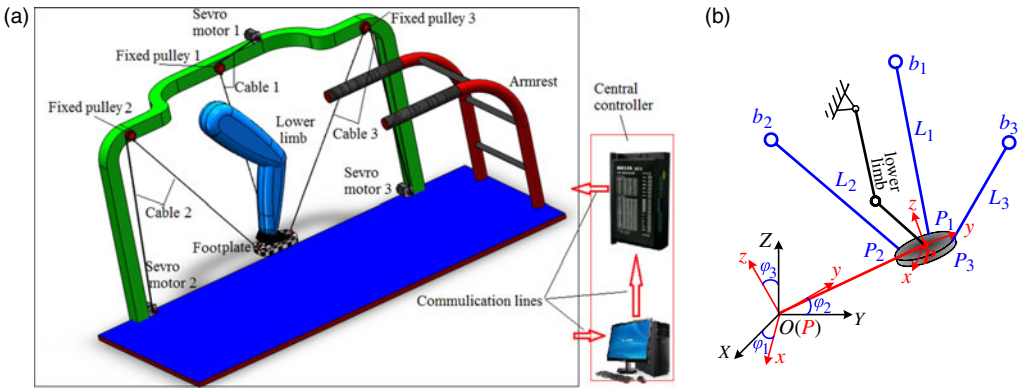

Fig. 1. Cable-driven lower-limb rehabilitation training robot: (a) one side model of CLLRTR; (b) simplified model diagram of one side of CLLRTR.

2. Configuration of CLLRTR

CLLRTR is mainly used to restorative training for different levels of disability of the lower limb by controlling means of cables. The system of CLLRTR is shown in Fig. 1. The construction of this CLLRTR is symmetrical. Each side of CLLRTR is formed by three cables.

CLLRTR is composed of the cables, fixed pulleys, servo motors, and footplate (end-effector) that guide the motion of the leg during the rehabilitation training. The footplate is connected to the roller fixed on servo motor by means of cables and fixed pulleys, and each group of cables is driven by an independent servo motor, as shown in Fig. 1(a). The simplified model diagram of one side of CLLRTR is shown in Fig. 1(b). A fixed frame (O, X, Y, Z) is attached to the base of CLLRTR and is referred to as the base frame. A moving frame (P, x, y, z) is attached to the footplate, where P is the reference point that is positioned at the geometric centre of the footplate. Point b_i, at which the i^{th} $(i = 1, 2, 3)$ cable enters the spool of the i^{th} fixed pulley, is the position of the fixed pulley. Point P_i is a junction position between the i^{th} cable and the footplate. The i^{th} cable length is noted by L_i. The posture of the footplate is noted by the vector $[\varphi_1, \varphi_2, \varphi_3]^{\text{T}}$. The position of the footplate is described by using $\boldsymbol{P} = [x, y, z]^T$. In addition, the symbols describing of the important variables are shown in Table I.

3. Dynamics of CLLRTR

Assume that the motion of the footplate with n DOF is realized by the driving of m cables, and $m < n \leq 6$. This paper mainly studies the footplate with $n = 6$ DOF. Because the cable length of the rehabilitation robot is shorter and the cable inertia is smaller, the mass and elastic deformation of the cable, which has very little effect on the system, can be ignored. Referring to Fig. 1, the cable length can be written as:

$$L_i = \sqrt{(x_i - x_{pi})^2 + (y_i - y_{pi})^2 + (z_i - z_{pi})^2} \quad (i = 1, 2, \ldots, m) \tag{1}$$

https://doi.org/10.1017/S0263574720000879 Published online by Cambridge University Press

where (x_i, y_i, z_i) is the positions b_i in the base frame. (x_{pi}, y_{pi}, z_{pi}) is the position P_i in the base frame, and it can be written as:

$$\begin{bmatrix} x_{pi} \\ y_{pi} \\ z_{pi} \end{bmatrix} = \begin{bmatrix} x \\ y \\ z \end{bmatrix} + {}^{O}\boldsymbol{R}_{p} \begin{bmatrix} {}^{p}x_{pi} \\ {}^{p}y_{pi} \\ {}^{p}z_{pi} \end{bmatrix} \tag{2}$$

where $[{}^{p}x_{pi}, {}^{p}y_{pi}, {}^{p}z_{pi}]^T$ is the position P_i in the moving frame. The rotation matrix ${}^{O}\boldsymbol{R}_{P}$ can be written as:

$$\begin{aligned} {}^{o}\boldsymbol{R}_{P} &= R_z(\varphi_3) R_y(\varphi_2) R_x(\varphi_1) \\ &= \begin{bmatrix} \cos\varphi_3 & -\sin\varphi_3 & 0 \\ \sin\varphi_3 & \cos\varphi_3 & 0 \\ 0 & 0 & 1 \end{bmatrix} \begin{bmatrix} \cos\varphi_2 & 0 & \sin\varphi_2 \\ 0 & 1 & 0 \\ -\sin\varphi_2 & 0 & \cos\varphi_2 \end{bmatrix} \begin{bmatrix} 1 & 0 & 0 \\ 0 & \cos\varphi_1 & -\sin\varphi_1 \\ 0 & \sin\varphi_1 & \cos\varphi_1 \end{bmatrix} \end{aligned}$$

The desired motion of the footplate is realized by the driving of m cables. The generalized dynamical equation of CLLRTR can be obtained by the Newton–Euler equation:

$$\boldsymbol{AT} = \boldsymbol{b} \tag{3}$$

where $\boldsymbol{A}$ is the structure matrix, it can be written as:

$$A = \begin{bmatrix} \frac{x_1 - x_{p1}}{L_1} & \frac{x_2 - x_{p2}}{L_2} & \cdots & \frac{x_{\mathrm{m}} - x_{pm}}{L_{\mathrm{m}}} \\ \frac{y_1 - y_{p1}}{L_1} & \frac{y_2 - y_{p2}}{L_2} & & \frac{y_{\mathrm{m}} - y_{pm}}{L_{\mathrm{m}}} \\ \frac{z_1 - z_{p1}}{L_1} & \frac{z_2 - z_{p2}}{L_2} & & \frac{z_{\mathrm{m}} - z_{pm}}{L_{\mathrm{m}}} \\ \frac{(y_1 - y_{p1})\, x_{p1} + (z_1 - z_{p1})\, y_{p1}}{L_1} & \frac{(y_2 - y_{p2})\, x_{p2} + (z_2 - z_{p2})\, y_{p2}}{L_2} & & \frac{(y_{\mathrm{m}} - y_{pm})\, x_{pm} + (z_{\mathrm{m}} - z_{pm})\, y_{pm}}{L_{\mathrm{m}}} \\ \frac{(x_1 - x_{p1})\, z_{p1} + (z_1 - z_{p1})\, x_{p1}}{L_1} & \frac{(x_2 - x_{p2})\, z_{p2} + (z_2 - z_{p2})\, x_{p2}}{L_2} & & \frac{(x_{\mathrm{m}} - x_{pm})\, z_{pm} + (z_{\mathrm{m}} - z_{pm})\, x_{pm}}{L_{\mathrm{m}}} \\ \frac{(y_1 - y_{p1})\, x_{p1} + (x_1 - x_{p1})\, y_{p1}}{L_1} & \frac{(y_2 - y_{p2})\, x_{p2} + (x_2 - x_{p2})\, y_{p2}}{L_2} & & \frac{(y_{\mathrm{m}} - y_{pm})\, x_{pm} + (x_{\mathrm{m}} - z_{pm})\, y_{pm}}{L_{\mathrm{m}}} \end{bmatrix} \tag{4}$$

$$\boldsymbol{T} = [\boldsymbol{t}_1\ \boldsymbol{t}_2\ \cdots\ \boldsymbol{t}_m]^{\mathrm{T}} \tag{5}$$

$$\left[\boldsymbol{M}\ddot{\boldsymbol{x}}\ \ \boldsymbol{M}\ddot{\boldsymbol{y}}\ \ \boldsymbol{M}(\ddot{\boldsymbol{z}} - \boldsymbol{g})\ \ \boldsymbol{J_x}\ddot{\boldsymbol{\varphi}}_{\boldsymbol{1}}\ \ \boldsymbol{J_y}\ddot{\boldsymbol{\varphi}}_{\boldsymbol{2}}\ \ \boldsymbol{J_z}\ddot{\boldsymbol{\varphi}}_{\boldsymbol{3}}\right]^{\mathrm{T}} \tag{6}$$

where $\boldsymbol{t}_i > 0\ (i = 1, 2, \ldots, m)$ is the cable tension, $\boldsymbol{M}$ is the equivalent mass of the lower limb and the footplate. $\boldsymbol{J_x}$, $\boldsymbol{J_y}$, and $\boldsymbol{J_z}$ are the rotary inertia respectively around axis X, Y, Z. $\ddot{\boldsymbol{x}}$, $\ddot{\boldsymbol{y}}$, and $\ddot{\boldsymbol{z}}$ are the translational acceleration respectively among the directions X, Y, Z. $\boldsymbol{g}$ is the gravity acceleration. $\ddot{\boldsymbol{\varphi}}_{\boldsymbol{1}}$, $\ddot{\boldsymbol{\varphi}}_{\boldsymbol{2}}$, and $\ddot{\boldsymbol{\varphi}}_{\boldsymbol{3}}$ are the angle acceleration respectively around axis X, Y, Z.

4. Analysis of Workspace

4.1. Analysis of wrench enclosure

It is known that at least $n + 1$ cables are required to satisfy the principle of vector closure in n DOF CDPR system from the principle of vector closure.[27] Moreover, the principle of vector closure can ensure that the tension force of each cable is all positive, and there is a unique solution to any external wrench.

The under-constrained CLLRTR with a 6-DOF footplate is studied in the study. The gravity and the inertia forces generated by the equivalent mass will be treated as tensions generated by the virtual cables. Their unit vectors can be written as $\boldsymbol{e}_g$, $\boldsymbol{e}_x$, $\boldsymbol{e}_y$, $\boldsymbol{e}_z$. The dynamical Eq. (3) of CLLRTR can be expressed as:

$$\boldsymbol{J}_{+}\boldsymbol{T}_{+} = \boldsymbol{0} \tag{7}$$

https://doi.org/10.1017/S0263574720000879 Published online by Cambridge University Press

where,

$$\begin{cases} \boldsymbol{J}_+ = [\boldsymbol{A} \quad \boldsymbol{J}_w] \\ \boldsymbol{T}_+ = \left[\boldsymbol{t}_1 \quad \boldsymbol{t}_2 \cdots \boldsymbol{t}_{\mathrm{m}} \quad \boldsymbol{Mg} \quad \boldsymbol{Ma}_x \quad \boldsymbol{Ma}_y \quad \boldsymbol{Ma}_z\right]^{\mathrm{T}} \end{cases} \tag{8}$$

where $\boldsymbol{a}_x$, $\boldsymbol{a}_y$, and $\boldsymbol{a}_z$ are the translational acceleration of the footplate respectively among the directions X, Y, Z. $\boldsymbol{J}_w$ is the wrench matrix that is composed of the gravity and inertia forces:

$$\boldsymbol{J}_w = \left[\boldsymbol{J}_g \quad \boldsymbol{J}_x \quad \boldsymbol{J}_y \quad \boldsymbol{J}_z\right] = \begin{bmatrix} \boldsymbol{e}_g & \boldsymbol{e}_x & \boldsymbol{e}_y & \boldsymbol{e}_z \\ \boldsymbol{0} & \boldsymbol{0} & \boldsymbol{0} & \boldsymbol{0} \end{bmatrix} \tag{9}$$

where $\boldsymbol{J}_g$, $\boldsymbol{J}_x$, $\boldsymbol{J}_y$, and $\boldsymbol{J}_z$ are the wrench of the footplate in the gravity, X, Y, and Z directions, respectively.

There are at most 3 DOF of the footplate can be dynamically controlled by adjusting the cable length when the number of the cable m is equal to 1 or 2. The formula $m \geq n + 1$ can be completely satisfied when the wrench matrix $\boldsymbol{J}_w$ is considered, that is, there is $1 \leq n \leq 3$ when m is equal to 1 or 2, and the system satisfies the conditions of the wrench closure. There are at most 6 DOF of the footplate can be dynamically controlled by adjusting the cable length when the number of cable $m \geq 3$. The formula $m \geq n + 1$ can be completely satisfied when the wrench matrix $\boldsymbol{J}_w$ is considered. Namely, there is $1 \leq n \leq 6$ when the number of cables $m \geq 3$, and the system satisfies the conditions of the wrench closure. The under-constrained CLLRTR satisfies the $m \leq n$, hence, the robot also satisfies the conditions of the wrench closure formula $m \geq n + 1$ when $m \geq 3$ and $3 < n \leq 6$. In summary, the 6-DOF CLLRTR can guarantee and meet the conditions of the wrench closure when the number of the driving cables m meets $3 \leq m \leq n$.

Based on the multi-finger friction-free grab model and the convex set theory,[26] the convex conditions to judge the wrench closure of the 6-DOF CLLRTR with m cables can be obtained:

(1) The cable-driven wrench is closure.
(2) The column of matrix $\boldsymbol{J}_+$ can be positive projected onto $\mathbf{R}^n$.
(3) The neighbouring region of the origin is contained in the convex packet of $\{\boldsymbol{J}_i\}$.
(4) There is no vector $\boldsymbol{\eta} \in \mathbf{R}^n$, and $\boldsymbol{\eta} \neq 0$ to meet all $\boldsymbol{\eta}\boldsymbol{J}_i \geq 0$, $i = 1, 2, \ldots, m$.

The above descriptions about the four conditions are all equivalent. The condition (4) has a practical significance for the calculation application. The vector $\boldsymbol{\eta}$ can be obtained based on the column of matrix $\boldsymbol{J}_+$: the support plane is formed by the two arbitrary selected column vectors from matrix $\boldsymbol{J}_+$, and the normal vector of the support plane formed by the two-column vectors $\boldsymbol{J}_i$ and $\boldsymbol{J}_j$ can be expressed by using $\boldsymbol{\eta}_{ij}$.

4.2. Analysis and solution of workspace

There are two methods to solve and analyze the workspace of the parallel robot: the analytical method and the numerical method. The analytical method can completely analyze the workspace of the parallel robot, because the configuration of this kind of parallel robot systems is very complex, and the system exists mechanical coupling. The analytical method is not a perfect solution to solve the position solution of the under-constrained parallel robot system. Hence, the analytical method does not apply to the workspace solution of this kind of spatial parallel robot system with a complex configuration. It is necessary to further consider the feasible range of changes in the cable tension, and the actual workspace of this kind of CDPR (i.e., the wrench feasible workspace) will be significantly smaller than that of the corresponding theoretical analysis. The numerical method has defects: a large amount of the calculation work and limited precision. However, the numerical method is easy to program, and can intuitively display the actual workspace of the system. Therefore, this paper will use the numerical method to solve the workspace of CLLRTR. On this basis, the stability of CLLRTR is analyzed.

The workspace of CLLRTR is the set of the spatial positions that can be reached by the end-effector (i.e., the centre of mass of the footplate) when the constraint conditions are met.[28] The

https://doi.org/10.1017/S0263574720000879 Published online by Cambridge University Press

workspace description of CLLRTR can be written as follows:

$$\boldsymbol{W} = \left\{(x, y, z, \varphi_1, \varphi_2, \varphi_3) \in \mathbf{R}^6 | g_0 (x, y, z, \varphi_1, \varphi_2, \varphi_3) \leqslant 0\right\} \tag{10}$$

where $\boldsymbol{W}$ is the generalized workspace of CLLRTR, $\mathbf{R}^6$ is the six-dimensional real number field, and $g_0(\bullet)$ represents the set of equations to the constraint conditions of CLLRTR.

The posture of the footplate is given using the Monte-Carlo method, the spatial position of the footplate and the cable length can be obtained through Eqs. (1) and (2). And the spatial position should satisfy the following conditions:

$$\begin{cases} \min(x_1, x_2, \ldots, x_{\mathrm{m}}) < x < \max(x_1, x_2, \ldots, x_{\mathrm{m}}) \\ \min(y_1, y_2, \ldots, y_{\mathrm{m}}) < y < \max(y_1, y_2, \ldots, y_{\mathrm{m}}) \\ \min(z_1, z_2, \ldots, z_{\mathrm{m}}) < z < \max(z_1, z_2, \ldots, z_{\mathrm{m}}) \end{cases} \tag{11}$$

Equation (3) can be regarded as a non-homogeneous linear equation set about $\boldsymbol{T}$ when the posture of the footplate is determined. There is rank $(\boldsymbol{A}) \leq \min(m, n)$ when the system does not occur in the singular motion. The under-constrained CLLRTR is studied in the paper, hence, there is rank $(\boldsymbol{A}) \leq m$. There is no solution to the equation if rank $(\boldsymbol{A}) \neq m$ rank $(\boldsymbol{A}, \boldsymbol{b})$, that is, the position does not satisfy the constraint conditions of CLLRTR. Else if rank $(\boldsymbol{A}) =$ rank $(\boldsymbol{A}, \boldsymbol{b}) = m$, the equation has a unique solution. Based on the Eq. (3), the cable tension can be expressed as:

$$\boldsymbol{T} = \boldsymbol{A}^{-1}\boldsymbol{b} \tag{12}$$

Else if rank $(\boldsymbol{A}) =$ rank$(\boldsymbol{A}, \boldsymbol{b}) < m$, the equation has infinitely many solutions. Based on the Moore–Penrose generalized inverse theory matrix, the minimal norm solution to the cable tension can be written as:

$$\boldsymbol{T}^* = \boldsymbol{A}^{\mathrm{T}} \left(\boldsymbol{A}\boldsymbol{A}^{\mathrm{T}}\right)^{-1} \boldsymbol{b} \tag{13}$$

The physical significance of the minimal norm solution of the cable tension in Eq. (13) is an optimal solution to the cable tensions that satisfy the constraint conditions of CLLRTR.

The cable can only provide the tension force, so the cable tension must be positive, and it cannot exceed the maximum allowable tension that the cable can withstand to ensure the safety and stability of the system, namely, the cable tension must meet the following conditions:

$$0 < t_i < T_{f\max} = \frac{T_{\lim}}{k} \tag{14}$$

where $T_{f\max}$ is the maximum allowable tension that the cable can withstand to ensure the safety and stability of the system, $T_{\lim}$ is the limit cable tension, and k is the safety coefficient which is subject to $1.5 < k < 2$.

The calculation steps of the workspace for CLLRTR are as follows:

(1) First of all, the structural parameters of CLLRTR are described. The posture of the footplate is randomly generated based on the Monte Carlo algorithm in the MATLAB environment. The rank $(\boldsymbol{A})$ and rank $(\boldsymbol{A}, \boldsymbol{b})$ are calculated by Eqs. (4) and (6).
(2) Judge whether the structural matrix meets rank $(\boldsymbol{A}) =$ rank$(\boldsymbol{A}, \boldsymbol{b}) = m$. If it does, and calculate the cable tension with Eq. (12), and go to step (4); if it does not, go to step (3).
(3) Judge whether the structural matrix meets rank $(\boldsymbol{A}) =$ rank$(\boldsymbol{A}, \boldsymbol{b}) < m$. If it does, calculate the cable tension through Eq. (13), and go to the step (4), if it is not and return to the step (1) to calculate the next position.
(4) Judge whether the cable tension meets $0 < t_i < T_{f\max} = \frac{T_{\lim}}{k}$, if it does, record this position. If it does not, return to the step (1) to calculate the next position.
(5) Repeat the steps (1)–(4) until the end.

https://doi.org/10.1017/S0263574720000879 Published online by Cambridge University Press

5. Dynamical Stability

The stability is the primary condition for the normal operation of the system. The dynamical stability refers to the ability of CLLRTR system to remain the original motion state when the system is subjected to external interference. The dynamical stability index of CLLRTR is given according to the Krasovski method, because of the complexity of the robot. The dynamical stability can't be determined by using the analytic method directly. Therefore, this paper only applies a numerical method to calculate the dynamical stability in the workspace, which is more valuable in the engineering application. The matrix eigenvalue decomposition method is used to calculate whether the stability margin condition is satisfied, and the stability evaluation index is proposed in the calculation process.

Combined with the Eqs. (1) and (3), the equation of the system can be written as:

$$\boldsymbol{f}^*(\boldsymbol{x}) = \boldsymbol{0} \tag{15}$$

where $x = [t_1\ t_2\ \cdots\ L_1\ L_2\ \cdots\ L_m\ \ddot{x}\ \ddot{y}\ \ddot{z}\ \ddot{\varphi}_1\ \ddot{\varphi}_2\ \ddot{\varphi}_3]^{\mathrm{T}}$, and $\boldsymbol{f}^*(\boldsymbol{x}) = \left[f_1(\boldsymbol{x}), f_2(\boldsymbol{x}), \ldots, f_{\mathrm{m}}(\boldsymbol{x}), f_{\mathrm{d1}}(\boldsymbol{x}), f_{\mathrm{d2}}(\boldsymbol{x}), \ldots, f_{\mathrm{d6}}(\boldsymbol{x})\right]^{\mathrm{T}}$, $f_i(\boldsymbol{x})$ can be obtained through the kinematics Eq. (1), $f_{\mathrm{d}j}(\boldsymbol{x})$ (j = 1,2, . . .,6) can be obtained through the dynamics Eq. (3). The second-order Taylor expansion at the equilibrium point $\boldsymbol{x}_0$ can be expressed as follows:

$$\boldsymbol{f}^*(\boldsymbol{x}) = \boldsymbol{f}^*(\boldsymbol{x}_0) + \left(\frac{\partial \boldsymbol{f}^*(\boldsymbol{x})}{\partial \boldsymbol{x}^{\mathrm{T}}}\right)_{\boldsymbol{x}_0}(\boldsymbol{x}-\boldsymbol{x}_0) + \frac{1}{2!}\frac{\partial}{\partial \boldsymbol{x}^{\mathrm{T}}}\left(\frac{\partial \boldsymbol{f}^*(\boldsymbol{x})}{\partial \boldsymbol{x}^{\mathrm{T}}}\right)_{\boldsymbol{x}_0}(\boldsymbol{x}-\boldsymbol{x}_0)^2 + R_n \tag{16}$$

Ignoring the high-order item R_n, Eq. (16) can be further written as follows:

$$\dot{x} = f(\boldsymbol{x}) \tag{17}$$

CLLRTR is a nonlinear system, and the dynamical stability of the kind system can be calculated according to the Krasovski method. The partial derivative equations for $\boldsymbol{x}$ on Eq. (17) can be written as:

$$\boldsymbol{J}(\boldsymbol{x}) = \frac{\partial \boldsymbol{f}(\boldsymbol{x})}{\partial \boldsymbol{x}^{\mathrm{T}}} \tag{18}$$

The defined Lyapunov function can be noted as:

$$V(\boldsymbol{x}) = f^{\mathrm{T}}(\boldsymbol{x}) f(\boldsymbol{x}) \tag{19}$$

There is:

$$\begin{aligned}\frac{\mathrm{d}V(\boldsymbol{x})}{\mathrm{d}t} &= \frac{\mathrm{d}f^{\mathrm{T}}(\boldsymbol{x})}{\mathrm{d}t} f(\boldsymbol{x}) + f^{\mathrm{T}}(\boldsymbol{x})\frac{\mathrm{d}f(\boldsymbol{x})}{\mathrm{d}t} \\ &= \left[\frac{\partial f(\boldsymbol{x})}{\partial \boldsymbol{x}^{\mathrm{T}}}\cdot\frac{\mathrm{d}\boldsymbol{x}}{\mathrm{d}t}\right]^{\mathrm{T}} f(\boldsymbol{x}) + f^{\mathrm{T}}(\boldsymbol{x})\left[\frac{\partial f(\boldsymbol{x})}{\partial \boldsymbol{x}^{\mathrm{T}}}\cdot\frac{\mathrm{d}\boldsymbol{x}}{\mathrm{d}t}\right] \\ &= f(\boldsymbol{x})\left[\boldsymbol{J}^{\mathrm{T}}(\boldsymbol{x}) + \boldsymbol{J}(\boldsymbol{x})\right] f^{\mathrm{T}}(\boldsymbol{x}) \\ &= f(\boldsymbol{x})\boldsymbol{F}(\boldsymbol{x}) f^{\mathrm{T}}(\boldsymbol{x})\end{aligned} \tag{20}$$

If $\boldsymbol{F}(\boldsymbol{x})$ is negative, that is, $\boldsymbol{F}(\boldsymbol{x}) < \boldsymbol{0}$, the cable tensions $t_i > 0$ ($i = 1, 2, \ldots, m$), so $\boldsymbol{x} \neq \boldsymbol{0}$, and it is known that the function $\boldsymbol{V}(\boldsymbol{x}) > 0$ from Eq. (19). Combined with the Eqs. (19) and (20), we can know $\frac{\mathrm{d}V(\boldsymbol{x})}{\mathrm{d}t} < 0$, and the system is asymptotically stable according to the Lyapunov stability theorem. Hence, there is,

$$\boldsymbol{F}(\boldsymbol{x}) = \boldsymbol{J}(\boldsymbol{x}) + \boldsymbol{J}^{\mathrm{T}}(\boldsymbol{x}) \tag{21}$$

If the matrix $\boldsymbol{F}(\boldsymbol{x})$ is negative, the system is gradually stable.

It further shows that the system is gradually stable on a large scale if the above function meets condition: when $\boldsymbol{x} \to \infty$, there is $\| f(\boldsymbol{x})\| \to \infty$. The system obviously meets this condition. Therefore, it is only necessary to determine whether the $\boldsymbol{F}(\boldsymbol{x})$ matrix is negative or not, then we can judge whether the system is stable.

https://doi.org/10.1017/S0263574720000879 Published online by Cambridge University Press

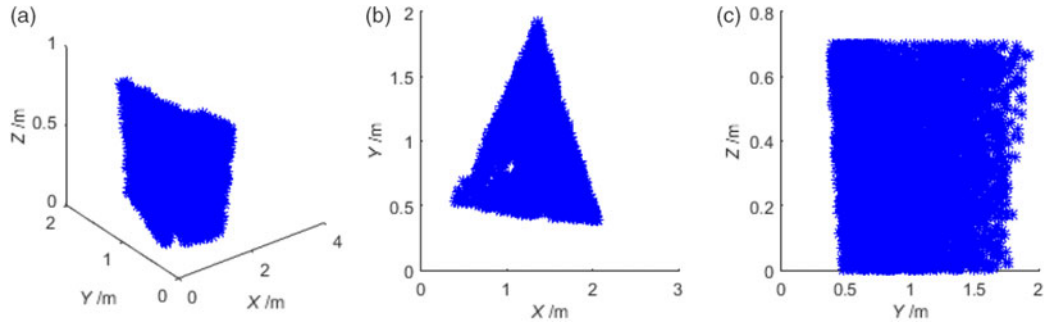

Fig. 2. The workspace of CLLRTR. (a) three-dimensional workspace (b) projections on the *XOY* plane (c) projections on the *YOZ* plane.

In the process of the calculation stability, the matrix eigenvalue decomposition method is used to judge whether the matrix $\boldsymbol{F}(\boldsymbol{x})$ is negative or not,

$$\boldsymbol{F}(\boldsymbol{x})\boldsymbol{V} = \boldsymbol{V}\boldsymbol{D} \tag{22}$$

$$\boldsymbol{V} = \begin{bmatrix} \boldsymbol{V}_1 & \boldsymbol{V}_2 & \cdots & \boldsymbol{V}_{\mathrm{m}} \end{bmatrix} \tag{23}$$

$$\boldsymbol{D} = \begin{bmatrix} \lambda_1 & & & \\ & \lambda_2 & & \\ & & \ddots & \\ & & & \lambda_{\mathrm{m}} \end{bmatrix} \tag{24}$$

Eq. (22) can be written as the form of Eq. (25) to solve eigenvalue of the matrix $\boldsymbol{D}$.

$$(\boldsymbol{F}(\boldsymbol{x}) - \boldsymbol{D}\boldsymbol{E}) = \boldsymbol{0} \tag{25}$$

where $\boldsymbol{D}$ is the eigenvalue matrix of $\boldsymbol{F}(\boldsymbol{x})$. $\boldsymbol{E}$ is a unit matrix. The column vector $\boldsymbol{V}_i$ of the matrix $\boldsymbol{V}$ is eigenvector that is corresponding to the eigenvalue λ_i of the matrix $\boldsymbol{F}(x)$. Due to $\boldsymbol{F}(x)$ is a symmetric matrix, the eigenvalue λ_i of the matrix $\boldsymbol{F}(x)$ is all real. If $\lambda_i < 0$, it shows that the matrix $F(x)$ is negative, that is, the motion of the system is stable; else if $\lambda_i \geq 0$, it shows that the matrix $\boldsymbol{F}(x)$ is not negative and the motion of the system is not stable or critical stable.

In order to evaluate the dynamical stability of CLLRTR in the workspace, the maximum value S of the eigenvalue λ_i is proposed to measure the stability degree of the motion, that is,

$$S = \max\{\lambda_1, \lambda_2, \ldots, \lambda_{\mathrm{m}}\} \tag{26}$$

The system is not stable or critical stable if $S \geq 0$, the system is stable if $S < 0$, and the smaller the value of S is, the better the dynamical stability degree of the system is.

6. Numerical Simulation and Experimental Analysis

6.1. Simulation analysis

The workspace of CLLRTR is simulated in the MATLAB environment, and the dynamical stability index in the workspace is calculated. The structure of CLLRTR is displayed in Fig. 1, and the parameters of the prototype are described as follows: the positions of the fixed pulleys are b_1(2.3, 0.42, 0.72) m, b_2(0.38, 0.48, 0.72) m, b_3(0.36, 2.0, 0.72) m. Assume the junctions between the footplate and the cables are vertices of a regular triangle, and the distance between the junctions P_i is $l = 0.15$ m. The force acted on the footplate by the lower limb is $F_m = 100$ N. The acceleration of the footplate are $a_X = a_Y = 0.001$ m/s^2, $a_Z = 0$. The variable range of the angle φ_3 is (−0.1 rad, 0.1 rad), and $\varphi_1 = \varphi_2 = 0$. The rotary inertia of the footplate are $J_x = 0.54$, $J_y = 0.26$, $J_z = 0.28$, respectively. The cable pretension $t_{\min} = 15$ N, and the cables maximum license tension $t_{\max} = 600$ N.

The workspace of the CLLRTR is shown in Fig. 2. Figure 2 shows that the workspace of CLLRTR is a similar triangular prism that is composed of three fixed pulleys and their projections on the *XOY* plane. The constraints of the cable pretension and the posture angle for the footplate make the volume

https://doi.org/10.1017/S0263574720000879 Published online by Cambridge University Press

Table II. The value of the coefficients.

Z/m	a_4	a_3	a_2	a_1	a_0
0.5	3.640	−16.517	29.068	−23.572	6.3355
0.6	3.3607	−15.483	27.855	−23.077	6.2161

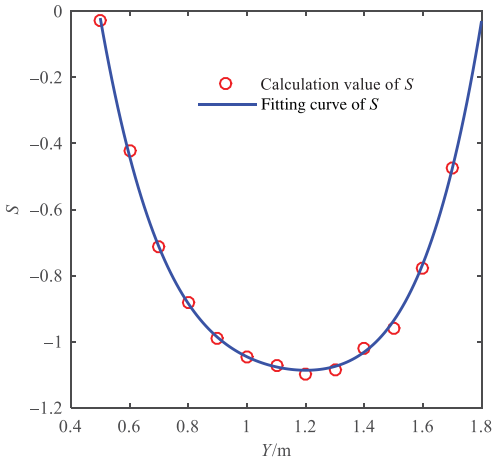

Fig. 3. The distribution of the stability evaluation index S on the line (1.225, y, 0.5) m.

of the workspace gradually increases from the bottom surface to the top surface. The range of S in the workspace is $S \in [-1.1486,\ -0.0254]$. It indicates that CLLRTR is stable in the workspace.

It is necessary to further analyze the distribution of the dynamical stability evaluation index S in the workspace. Assuming the posture angles of footplate $\varphi_1 = \varphi_2 = \varphi_3 = 0$, the distribution of the dynamical stability evaluation index S on the line (1.225, y, 0.5) m and (1.225, y, 0.6) m are calculated in the MATLAB environment, respectively. The four polynomial of the dynamical stability evaluation index S value is fitted by the least-squares method. The fitted four polynomials can be written as:

$$S = a_4 y^4 + a_3 y^3 + a_2 y^2 + a_1 y + a_0 \tag{27}$$

The values of the coefficients in the Eq. (27) are shown in Table II.

The distribution of the dynamical stability evaluation index S on the line (1.225, y, 0.5) m is shown in Fig. 3. The result shows that the S value becomes smaller firstly and then becomes larger with the increase of the y value. It indicates that the dynamical stability on the line (1.225, y, 0.5) m gradually improves firstly then gradually decreases with the increase of the y value, and the point of the best dynamical stability is at the midpoint of the line.

The distribution of the dynamical stability evaluation index S in the line (1.225, y, 0.6) m is shown in Fig. 4. The result shows that the variation trend of the dynamical stability evaluation index S in the line (1.225, y, 0.6) m is the same as in the line (1.225, y, 0.5) m. It indicates that the variation trend of the robot's dynamical stability in the line (1.225, y, 0.6) m is also the same as in the line (1.225, y, 0.5) m.

Since the structure of CLLRTR is symmetrical, the changing trend of the dynamical stability in the X-direction is the same as the changing trend in the Y-direction.

It shows that the dynamical stability of the central area is better than that of the boundary area in the same plane. The distribution of the cable tension is more uniform in the central area than in the boundary area, the stronger the ability to keep the motion state unchanged is, and the better the dynamical stability of CLLRTR is.

By comparing Fig. 4 with Fig. 3, we can know that the S value decreases gradually with the increase of the value z. Such as, the dynamical stability evaluation index $S = -1.086$ in the position (1.225, 1.21, 0.5) m, and $S = -1.195$ in the position (1.225, 1.21, 0.6) m, and it indicates that the lager the value z is, the better the dynamical stability of CLLRTR is. Because the larger the value z is, the larger the cables tensions will be, and the larger the stiffness of the robot system is. And it will

https://doi.org/10.1017/S0263574720000879 Published online by Cambridge University Press

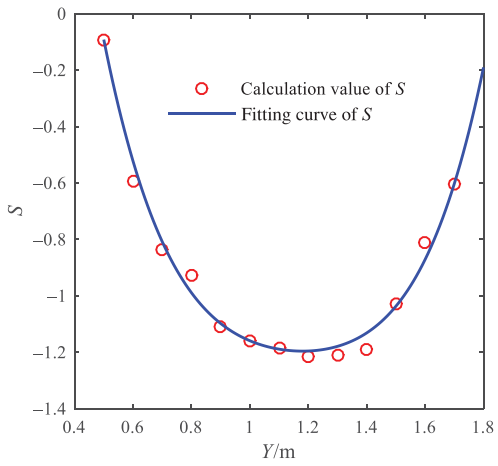

Fig. 4. The distribution of the stability evaluation index S on the line (1.225, y, 0.6) m.

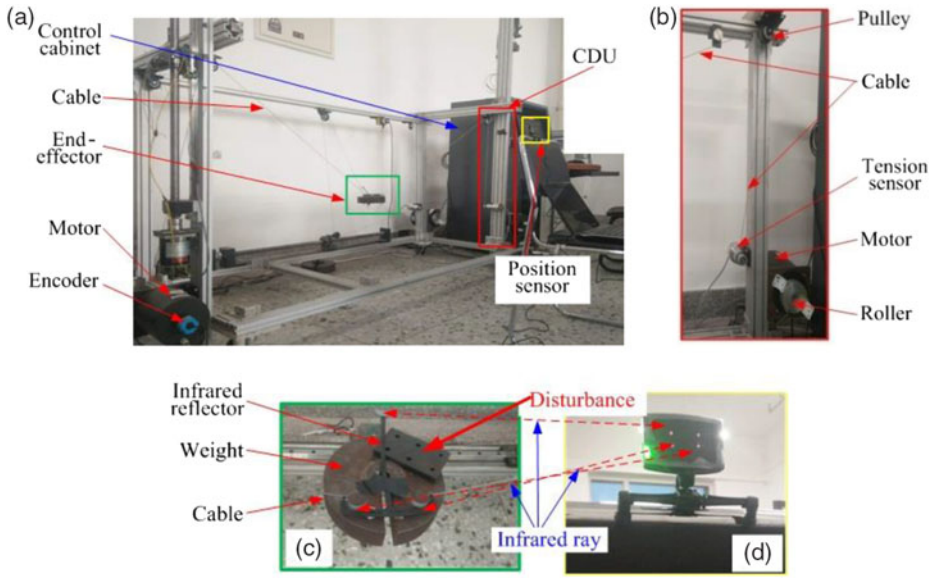

Fig. 5. Experimental system of CLLRTR. (a) Experimental system of CLLRTR (b) CDU (c) End-effector (d) Position sensor.

lead the robot system to have a stronger ability to resist external interferences, which will make the motion of CLLRTR more stable.

In summary, the dynamical stability of the central area is better than that of the boundary area, and the dynamical stability is better in the upper area than in the lower area of the workspace of CLLRTR. Therefore, in the practical application, at the premise of satisfying the motion function of the lower limbs rehabilitation training, the motion trajectory of the footplate should be planned in the centre and upper area of the workspace as far as possible. It lays a foundation for the trajectory planning of the lower-limb rehabilitation training robot.

6.2. Experimental study

The experimental system of CLLRTR with three cables was built to analyze the dynamical stability of CLLRTR system, as shown in Fig. 5(a). The experimental system consists of three groups the cable-driven units (CDU), end-effector, control cabinet (including the control card and drivers), position sensor, and framework. The CDU is shown in Fig. 5(b), the torque motor (Model: 130LYX30N) integrates the photoelectric encoder (Model: BXD-13A-500BM-G05L) and roller. One end of the cable is attached to the roller across the tension sensor and the pulley. The other end of the cable is attached to the end-effector. The tension sensors are used to detect the cable tension. The end-effector is shown in Fig. 5(c). The end-effector is a weight (the mass is 10 kg), and a disturbance (the mass is 1 kg)

https://doi.org/10.1017/S0263574720000879 Published online by Cambridge University Press

is installed on the edge of the weight to generate external interference force. An infrared reflector bracket that is installed on the centre of the weight is used to collect the position of the end-effector by combining itself with the position sensor. As shown in Fig. 5(d), the position sensor emits the infrared rays, and the infrared rays are reflected by the infrared reflector bracket installed on the end-effector. Then the position sensor detects the infrared rays and calculates the position of the end-effector. The correctness of the dynamical stability can be verified by testing the ability of CLLRTR to maintain the motion state of the end-effector with the external disturbance in the different motion trajectories.

The parameters of the experimental system are the same as the simulation parameters.

6.2.1. Experiment A1. Experiment A1 is mainly used to verify the distribution of the dynamical stability in the vertical direction of the workspace and the correctness of the theoretical analysis. Therefore, the vertical midline of the workspace is selected as the motion trajectory A1 of the end-effector in the experiment A1, as follows,

$$\begin{cases} \begin{cases} x = 840 \\ y = 250 \\ z = 200 + 25t \end{cases} & (0 \leqslant t \leqslant 10\text{s, A1}) \\ \begin{cases} \varphi_1 = \varphi_2 = \varphi_3 = 0 & \text{(A1-1)} \\ \begin{cases} \varphi_1 = \varphi_2 = \pi \sin(\pi t/10)/12 \\ \varphi_3 = 0 \end{cases} . & \text{(A1-2)} \end{cases} \end{cases} \tag{28}$$

The angles of the end-effector $\varphi_1 = \varphi_2 = \varphi_3 = 0$ in the experiment A1-1, and $\varphi_1 = \varphi_2 = \pi \sin(\pi t/10)/12$, $\varphi_3 = 0$ in the experiment A1-2. The effect law of the angles of the end-effector on the dynamical stability of CLLRTR can be studied by experiment A1-1 and experiment A1-2.

The experimental data of the experiment A1 are shown in Fig. 6 in the interference of the disturbance. It can be seen that the motion errors of the position and posture angle gradually increases with the increase of the value Z (or times in Fig. 6) in the experiment A1-1, and maximum error values are max[|ΔX|, |ΔY|, |ΔZ|] = [0.2912, 4.987, 8] mm, max[|$\Delta\varphi_1$|, |$\Delta\varphi_2$|, |$\Delta\varphi_3$|] = [0.64, 0.6, 0.38] degree; the motion errors in the experiment A1-2 are larger than in the experiment A1-1. In the experiment A1-2, the position errors began to increase after about 1.7 s, and began to decrease gradually after about 7.3 s. Due to the inertia of the end-effector, the maximum motion errors of the angles φ_1 and φ_2 occur at approximately 1.7 and 7.3 s; the maximum error values are max[|ΔX|, |ΔY|, |ΔZ|] = [3.7, 6.14, 19.67] mm, and max[|$\Delta\varphi_1$| , |$\Delta\varphi_2$| , |$\Delta\varphi_3$|] = [6.002, 5.69, 0.6] degree in the experiment A1-2. The volatility of the cable tensions is significantly larger in the experiment A1-2 than in the experiment A1-1. The experimental results show that, in the vertical direction, the ability of the system to resist external interference gradually increases with the increase of Z value, and the ability to resist external interference will be decreased with the increase of the posture angles of the end-effector.

In the course of rehabilitation training, the movement of the experiment A1-1 can be considered as stable, for the patients with more serious initial training, and the movement in the experiment A1-2 can be considered as unstable. But the movement in the experiment A1-1 and in the experiment A1-2 can be considered as stable for the patients with certain motion ability and in the lower limb strength rehabilitation training.

6.2.2. Experiment A2. Experiment A2 is mainly used to verify the distribution law of the dynamical stability in the horizontal section of the workspace. Therefore, the motion trajectory A2 of the end-effector in the experiment A2 can be expressed as,

$$\begin{cases} x = 50\cos(\pi t/10) + 840 \\ y = 50\sin(\pi t/10) + 250 \\ z = 400 \\ \varphi_1 = \varphi_2 = \varphi_3 = 0 \end{cases} \quad (0 < t \leqslant 20\text{s}) \tag{29}$$

https://doi.org/10.1017/S0263574720000879 Published online by Cambridge University Press

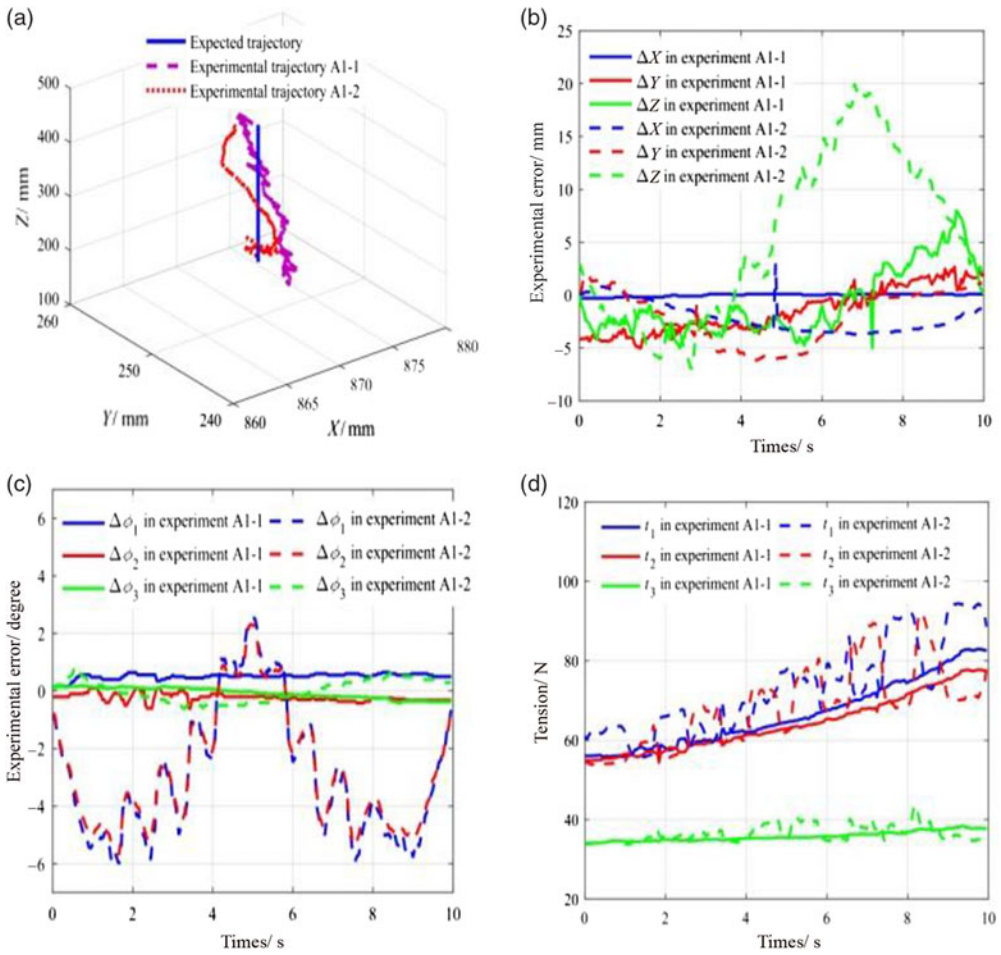

Fig. 6. The experimental data of the experiment A1. (a) The experimental trajectories (b) The motion errors of X, Y and Z (c) The motion errors of φ_1, φ_2 and φ_3 (d) The cable tensions.

$$\begin{cases} x = 100\cos((t-30)\pi/10) + 840 \\ y = 100\sin((t-30)\pi/10) + 250 \\ z = 400 \\ \varphi_1 = \varphi_2 = \varphi_3 = 0 \end{cases} \quad (0 < t \leqslant 20\text{s}) \tag{30}$$

Eqs. (29) and (30) represent the motion trajectories of the experiment A2-1 and experiment A2-2, respectively.

The experimental data of the experiment A2 are shown in Fig. 7 in the interference of disturbance. It can be seen that the motion errors in the experiments A2-1 and A2-2 have a certain periodicity, because the distance between the circular trajectory and the boundary of the workspace shape determined by the configuration of the robot is periodic. The motion error of the experiment A2-1 is significantly smaller than that of the experiment A2-2. And maximum error values are max[|ΔX|, |ΔY|, |ΔZ|] = [26.53, 15.43, 4] mm, max[|$\Delta\varphi_1$|, |$\Delta\varphi_2$|, |$\Delta\varphi_3$|] = [1.7, 1.3, 0.8] degree in the experiment A2-1; maximum error values are max[|ΔX|, |ΔY|, |ΔZ|] = [45.2, 53.59, 22] mm, max[|$\Delta\varphi_1$|, |$\Delta\varphi_2$|, |$\Delta\varphi_3$|] = [7.1, 6.12, 4.11] degree in the experiment A2-2. The volatility of the cable tensions is significantly larger in the experiment A2-2 than in the experiment A2-1. The experimental results show that, in the horizontal section, the ability of the system to resist external interference is stronger in the central area than in the boundary area of the workspace.

In the course of rehabilitation training, the movement of the experiment A2-1 can be considered as stable, for the patients with more serious initial training, and the movement in the experiment A2-2 can be considered as unstable. But the movement in the experiment A2-2 can be considered as stable for the patients with certain motion ability and in the lower limb strength rehabilitation training.

https://doi.org/10.1017/S0263574720000879 Published online by Cambridge University Press

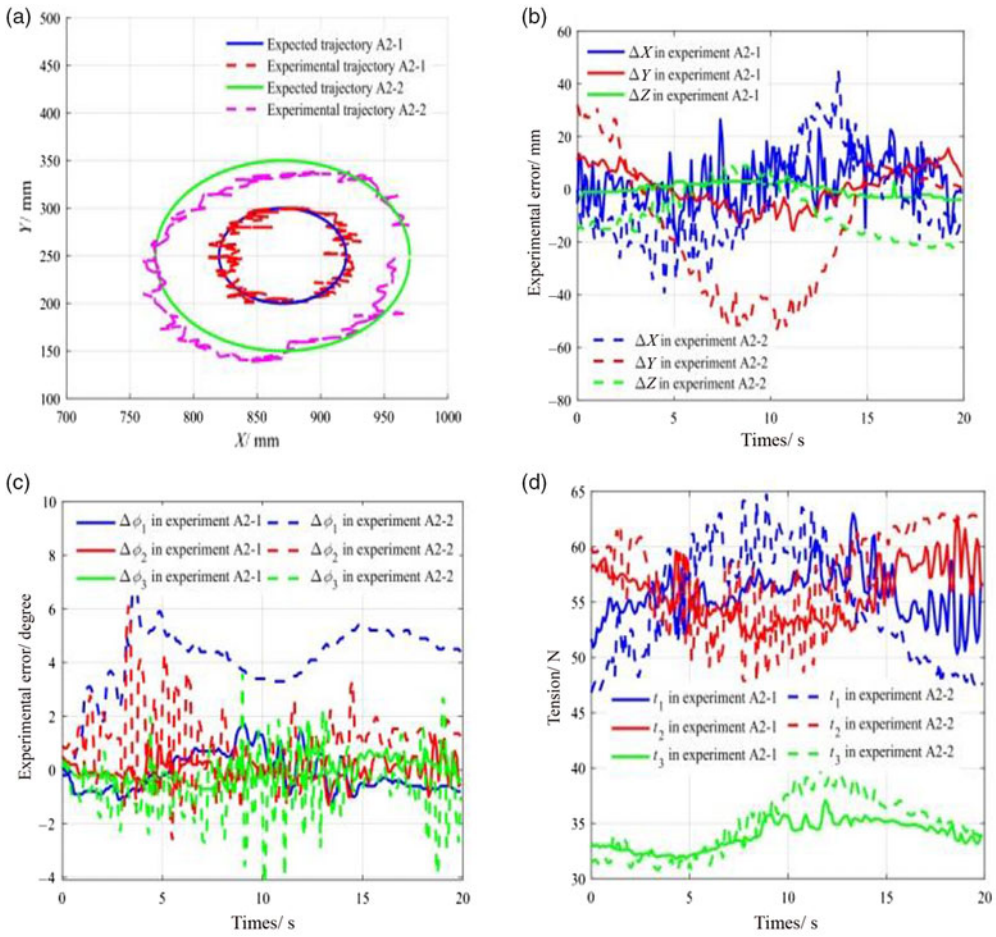

Fig. 7. The experimental data of the experiment A2. (a) The experimental trajectories (b) The motion errors of X, Y and Z (c) The motion errors of φ_1, φ_2 and φ_3 (d) The cable tensions.

The distribution of the dynamical stability index of CLLRTR was verified by the above experiments A1 and A2. The experimental results are consistent with the analysis results, it indicates that the dynamical stability evaluation method is correct and can be used to evaluate the dynamical stability of CLLRTR.

7. Conclusion

This paper introduces a CLLRTR that can accomplish different space rehabilitation training. The dynamical stability of CLLRTR is discussed. The solution to the wrench closure of this kind under-constrained system is presented by using the virtual cables method, and the dynamical stability index of CLLRTR is discussed by the Krasovski method. The evaluation index of the dynamical stability is proposed based on the matrix eigenvalue decomposition method. The experimental results of a specific CLLRTR show that the dynamical stability of the central area is better than that of the boundary area, and the dynamical stability of CLLRTR is better in the upper area of the workspace than in the bottom area in the whole workspace. Moreover, this research can be extended to do with the incomplete restrained, complete restrained, and redundant restrained CDPRs. The results provide a reference for designing a new CDU to improve the dynamical stability of CLLRTR. It will make the fact that patients can receive safe and effective rehabilitation training.

Acknowledgments

The authors disclosed receipt of the following financial support for the research, authorship, and/or publication of this article: This project is supported by the National Natural Science Foundation of

China (51405095), Natural Science Foundation of Heilongjiang Province, China (LH2019E032), and Postdoctoral Scientific Research Fund of Heilongjiang (LBH-Q15030), Fundamental Research Fund for the Central Universities (3072020CF0706).

References

1. B. Chen, H. Ma, L. Yin, F. Gao, K. M. Chan, S. W. Law, L. Qin and W. H. Liao, "Recent developments and challenges of lower extremity exoskeletons," *J. Orthop. Transl.* **5**(SI), 26–37 (2016).
2. Y. L. Wang, K. Y. Wang, W. Y. Zhao, W. L. Wang, Z. Han and Z. X. Zhang, "Effects of single crouch walking gaits on fatigue damages of lower extremity main muscles," *J. Mech. Med. Biol.* **19**(7), 1940046: 1–12 (2019).
3. D.-w. Jin, L.-h. Ji, J.-k. Yang and J.-c. Zhang, "Application of bio-mechanology research in rehabilitation engineering," *Chin. J. Rehabil. Med.* **25**(1), 61–64 (2010).
4. K.-y. Wang, P.-c. Yin, H.-p. Yang and L. Wang, "Motion planning of rigid chain for rigid–flexible coupled robot," Int. *J. Adv. Robot. Syst.* **15**(3), 1–10 (2018).
5. K.-Y. Wang, C.-B. Di, X.-Q. Tang and S. Zhang, "Modeling and simulation to muscle strength training of lower limbs rehabilitation robots," *Adv. Mech. Eng.* **7**(1), 1–8 (2015).
6. A. Ming and T. Higuchi, "Study on multiple degree of freedom positioning mechanisms using wires (part1): Concept, design and control," *Int. J. Jpn. Soc. Precis. Eng.* **28**(2), 131–138 (1994).
7. T.-f. Yan, M. Cempini, C. M. Oddo and N. Vitiello, "Review of assistive strategies in powered lower-limb orthoses and exoskeletons," *Robot. Auton. Syst.* **64**, 120–136 (2015).
8. S.-z. Liu, J.-s. Dai, G. Shen, A.-m. Li, G.-h. Cao, S.-z Feng and D.-y. Meng, "Dynamic analysis of spatial parallel manipulator with rigid and flexible couplings," *J. Central South Univ.* **24**(4), 840–853 (2017).
9. A. Berti, J.-P. Merlet and M. Carricato, "Solving the direct geometrico-static problem of underconstrained cable-driven parallel robots by interval analysis," *Int. J. Robot. Res.* **35**(6), 723–739 (2015).
10. X. Li, Y.-p. Pan, G. Chen and H.-y. Yu, "Multi-modal control scheme for rehabilitation robotic exoskeletons," *Int. J. Robot. Res.* **36**(5–7), 759–777 (2017).
11. D.-w. Jin, L.-h. Ji, J.-k. Yang and J.-c. Zhang, "Application of bio-mechanology research in rehabilitation engineering," *Chin. J. Rehabil. Med.* **25**(1), 61–64 (2010).
12. S. Hesse, H. Schmidt and C. Werner, "'Machines to support motor rehabilitation after stroke: 10 years of experience in berlin," *J. Rehabil. Res. Dev.* **43**(5), 671–678 (2006).
13. J. L. Emken, J. H. Wynne, S. J. Harkema and D. J. Reinkensmeyer, "A robotic device for manipulating human stepping," *IEEE Trans. Robot.* **22**(1), 185–189 (2006).
14. H. Schmidt, D. Sorowka, S. Hesse and R. Bernhardt "Development of a robotic walking simulator for gait rehabilitation," *Biomed. Tech. (Berl.)* **48**(10), 281–286 (2003).
15. K. X. Khor, H. A. Rahman, S. K. Fu, L. S. Sim, C. F. Yeong and E. L. M. Su, "A novel hybrid rehabilitation robot for upper and lower limbs rehabilitation training," *Proc. Comput. Sci.* **11**(42), 293–300 (2014).
16. G. Abbasnejad, J. Yoon and H. Lee, "Optimum kinematic design of a planar cable-driven parallel robot with wrench-closure gait trajectory," *Mech. Mach. Theory* **99**, 1–18 (2016).
17. H. Yuan, E. Courteille, M. Gouttefarde and P. E. Herve, "Vibration analysis of cable-driven parallel robots based on the dynamic stiffness matrix method," *J. Sound Vibr.* **394**, 527–544 (2017).
18. J. Yang, H. Su, Z. J. Li, D. Ao and R. Song, "Adaptive control with a fuzzy tuner for cable based rehabilitation robot," *Int. J. Cont. Automat. Syst.* **14**(3), 865–875 (2016).
19. S. Qian, B. Zi, W.-W. Shang and Q. S. Xu, "A review on cable-driven parallel robots," *Chin. J. Mech. Eng.* **31**(1), 66–77 (2018).
20. H. Lamine, S. Bennour and L. Romdhane, "Design of cable-driven parallel manipulators for a specific workspace using interval analysis," *Adv. Robot.* **30**(9), 585–594 (2016).
21. H. Kino, T. Yoshitake, R. Wada, K. Tahara and K. Tsuda, "3-DOF planar parallel-wire driven robot with an active balancer and its model-based adaptive control," *Adv. Robot.* **32**(14), 766–777 (2018).
22. Y. Lu, L. Yang, L.-j. Zhang, N.-j. Ye and Y.-l. Wang, "Dynamics analysis of a novel 5-DoF parallel manipulator with couple-constrained wrench," *Robotica* **36**(10), 1421–1435 (2018).
23. P. M. Bosscher and I. Ebert-UphoffImme, "A Stability Measure for Under-constrained Cable-Driven robots," **In:** *IEEE International Conference on Robotics and Automation* (2004) pp. 4943–4949.
24. N. Michael, J. Fink and V. Kumar, "Cooperative manipulation and transportation with aerial robots," *Auton. Robot* **30**(1), 73–86 (2011).
25. Y. L. Wang, K. Y. Wang, W. L. Wang, P. C. Yin and Z. Han, "Appraise and analysis of dynamical stability of cable-driven lower limb rehabilitation training robot," *J. Mech. Sci. Tech*. **33**(11), 5461–5472 (2019).
26. S. Behzadipour and A. Khajepour, "Stiffness of cable-based parallel manipulators with application to stability analysis," *J. Mech. Des.* **128**(1), 303–310 (2006).
27. Y.-h. Liang, *Research on Solution Method and Performance of the Workspace of Redundant Cable-Driven Parallel Robots* (Xidian University, Xi'an, 2010) (in Chinese).
28. C. Su, J. N. Ye, W. Li, W.C. Ding and Z. G. Zhao, "Analysis of dynamical workspace for under-constrained coordinate suspending system with multi-robots," *J. Shanghai Jiaotong Univ.* **53**(2), 225–231 (2019).